Physics of Fluids

RESEARCH ARTICLE | JUNE 18 2024

A general framework for the design of efficient passive pitch systems

Shūji Ōtomo ; Stefano Gambuzza ; Yabin Liu ; Anna M. Young ; Riccardo Broglia ; Edward D. McCarthy ; Ignazio Maria Viola

Check for updates

Physics of Fluids 36, 067122 (2024)
https://doi.org/10.1063/5.0212626

View Online
Export Citation

Articles You May Be Interested In

Helicopter aural detection as a function of reduced main rotor advancing blade tip Mach numbers

J. Acoust. Soc. Am. (October 1992)

Filamentation of unstable vortex structures via separatrix crossing: A quantitative estimate of onset time

Phys. Fluids (February 1989)

Topology and transport in generalized helical flows

Physics of Fluids (November 2021)

27 January 2026 08:52:58

AIP Advances
Why Publish With Us?
21DAYS average time to 1st decision
OVER 4 MILLION views in the last year
INCLUSIVE scope
Learn More
AIP Publishing

AIP Publishing

Physics of Fluids ARTICLE pubs.aip.org/aip/pof

A general framework for the design of efficient passive pitch systems

Cite as: Phys. Fluids **36**, 067122 (2024); doi: 10.1063/5.0212626
Submitted: 5 April 2024 · Accepted: 29 May 2024 ·
Published Online: 18 June 2024

View Online Export Citation CrossMark

Shūji Ōtomo,[1,2] Stefano Gambuzza,[1] Yabin Liu,[1] Anna M. Young,[3] Riccardo Broglia,[4] Edward D. McCarthy,[5] and Ignazio Maria Viola[1,a)]

AFFILIATIONS

[1]School of Engineering, Institute for Energy Systems, University of Edinburgh, Edinburgh EH9 3FB, United Kingdom
[2]Department of Mechanical Systems Engineering, Tokyo University of Agriculture and Technology, Tokyo 184-8588, Japan
[3]Department of Mechanical Engineering, University of Bath, Bath BA2 7AY, United Kingdom
[4]CNR-INM, Institute of Marine Engineering, National Research Council, Rome 00128, Italy
[5]School of Engineering, Institute for Materials and Processes, University of Edinburgh, Edinburgh, Robert Stevenson Road, EH9 3FB Scotland, United Kingdom

[a)]Author to whom correspondence should be addressed: i.m.viola@ed.ac.uk

ABSTRACT

Mitigating the impact of variable inflow conditions is critical for a wide range of engineering systems such as drones or wind and tidal turbines. Passive control systems are of increasing interest for their inherent reliability, but a mathematical framework to aid the design of such systems is currently lacking. To this end, in this paper a two-dimensional rigid foil that passively pitches in response to changes in the flow velocity is considered. Both an analytical quasi-steady model and a dynamic low-order model are developed to investigate the pivot point position that maximizes unsteady load mitigation. The paper focuses on streamwise gusts, but the proposed methodology would apply equally to any change in the inflow velocity (speed and/or direction). The quasi-steady model shows that the force component in any arbitrary direction can be kept constant if the pivot lies on a particular line, and that the line coordinates depend on the gust and the foil characteristics. The dynamic model reveals that the optimum distance of the pivot location from the foil increases with decreasing inertia. For a foil at small angles of incidence, the optimum pivot point is along the extended chord line. This knowledge provides a methodology to design optimum passively pitching systems for a plethora of applications, including flying and swimming robotic vehicles, and provides new insights into the underlying physics of gust mitigation.

© 2024 Author(s). All article content, except where otherwise noted, is licensed under a Creative Commons Attribution (CC BY) license (https://creativecommons.org/licenses/by/4.0/). https://doi.org/10.1063/5.0212626

27 January 2026 08:52:58

I. INTRODUCTION

Unsteady load management is crucial across many engineering disciplines, including the operation of small unmanned aerial vehicles (UAVs), which are significantly affected by environmental factors,[1–5] and in the mitigation of vibration and noise in aircraft and rotorcraft,[6–11] as well as in enhancing the efficiency and durability of wind and hydrokinetic turbines.[12–14] In comparison with larger aircraft, small UAVs face unique challenges in terms of control, flight stability, efficiency, and resilience, due to their lower inertia and thus increased vulnerability to disturbances such as gusts and atmospheric turbulence.[15–20] The use of UAVs in urban areas and under extreme weather conditions underscores the necessity for developing efficient systems to handle unsteady load fluctuations.

Actively controlled lift surfaces, such as trailing edge flaps, are standard,[21] while passive load alleviation mechanisms are less common, although they are gaining attention due to their inherent reliability and zero energy demand.[22–25] The natural world offers exemplary models of passive musculoskeletal adjustments, as seen in birds and insects, whose flight stability in turbulent conditions far surpasses that of human-made flyers. These creatures employ a mix of active and passive mechanisms to maintain position and velocity and to counteract the effects of wind gusts and lulls.[26–31] The kestrel's (*Falco tinnunculus*) ability to stabilize its gaze relative to the earth while hovering has intrigued both scientists and bird enthusiasts alike.[32–35] Distinguishing between active and passive responses to unsteady loads remains challenging, yet recent findings indicate a widespread reliance

© Author(s) 2024

on passive adaptations for this purpose.[36–40] The degree to which engineering systems can emulate these biological responses to mitigate load fluctuations, given the complexity of factors involved, including diverse wing shapes and gust profiles, is an ongoing area of investigation.

By analyzing a simplified two-dimensional foil model, free to adjust passively to changes in flow velocity and direction, we can isolate the essential physics of passive load mitigation. This analysis sheds light on the limits and potential of passive mechanisms for load alleviation, guides the interpretation of biological adaptations in nature, and informs the design of more effective and reliable engineering solutions for unsteady load challenges. This paper deliberately abstains from delving into specific application details, focusing instead on findings with broad implications across various design scenarios.

The manuscript is structured to begin with a formal definition of the passive pitch system (Sec. II) and a quasi-steady analysis of the initial and final state of the system for an arbitrary change in the free-stream speed and/or direction (Sec. III). It then progresses to the description of the dynamic low-order model (Sec. IV) and its application to streamwise gusts to investigate the optimal kinematics and pivot point location (Sec. V). It concludes by summarizing key outcomes and drawing conclusions (Sec. VI).

II. MODEL DEFINITION

Consider a two-dimensional rigid foil in an incompressible flow that rotates in response to a change in the magnitude and direction of the free-stream velocity (Fig. 1). The initial flow velocity is uniform and constant and exerts a constant fluid force on the foil, which is a function of the foil angle of attack. Then, the velocity varies over a transitory period to a different uniform velocity, which is kept constant until the foil position and fluid force converge to a new constant value.

For a constant free-stream velocity, the foil is held in position by an externally applied torque around the center of rotation, point P on Fig. 1, hereafter the pitching axis. The foil response is entirely passive: the torque is not adjusted based on the state of the system. In a biological system, the torque represents the musculoskeletal tension exerted on a joint. In an engineering system, the torque could be provided by a torsional spring. For example, Gambuzza *et al.*[41] considered a tidal turbine blade free to pitch around its spanwise axis, with a torsional spring around the axis. The large preload of the spring resulted in approximately constant torque, and the system allowed mitigation of the thrust and power fluctuations experienced by the turbine.

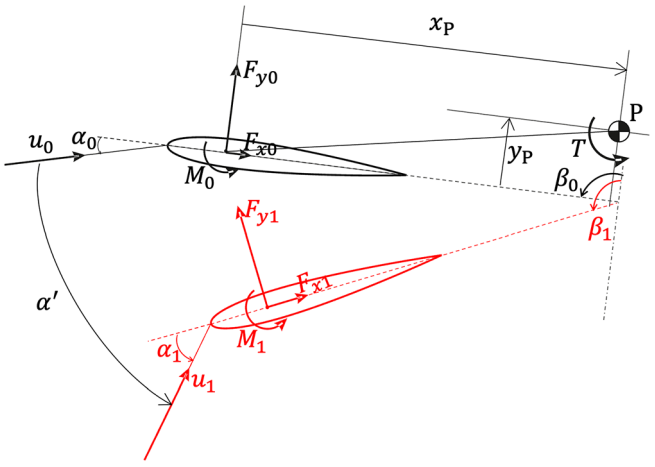

FIG. 1. Schematic diagram of the foil with relevant angles of attack (α), non-dimensional moments (M) around the quarter chord, and chordwise (F_x) and chord normal (F_y) forces, and the externally applied torque (T), all defined positive as in the figure. The freestream speed and direction change from u_0, α_0 to $u_1, \alpha_1 = \alpha_0 + \alpha'$ in the earth-fixed frame of reference. The foil rotates around the pivot P.

A bird wing is likely to both translate upward and backward and rotate around, for instance, its spanwise axis in response to a gust. At every instant, the combination of a rotation and a translation can be defined as a single rotation around a center of rotation. Therefore, while we consider some cases with centers of rotation that are far from the wing, a real mechanism could be made more compact by combining a rotation about a closer pitching axis with an additional translation to generate the same overall motion.

In this paper, we limit our study to fixed centers of rotation over the entire dynamic response period. Hence, for example, the foil cannot first translate and then rotate. Furthermore, we note that any in-plane translation of a rigid body is equivalent to a pure rotation around a center infinitely far from the body. For example, a horizontal translation is equivalent to a pure rotation around a center at an infinite distance above or below the foil. Similarly, a vertical translation of the foil is equivalent to a pure rotation around a center at an infinite distance left or right of the foil. However, a pure translation is not a physical solution because a rotation is necessary for the foil to change its angle of attack and reach a final equilibrium position.

III. QUASI-STEADY ANALYSIS

Consider a foil subject to an instantaneous freestream velocity having absolute value $\hat{u}$ at an angle α with the foil chord (Fig. 1). The foil is hinged around a pivot P at position $\mathbf{x}_P = (x_P, y_P)$ so that the only motion that is allowed is a rigid rotation around P.

All dimensional quantities are overlined with a caret denoted as $\hat{}$ and are made non-dimensional by using the fluid density $\hat{\rho}$, the foil chord $\hat{c}$, and the freestream speed at the initial state $\hat{u}_0$, as characteristic density, length, and velocity, respectively.

The foil chord forms an angle β with an arbitrary direction in the plane (Fig. 1), which is positive if a counterclockwise rotation is necessary to move from the arbitrary direction to the chord. We define, for this foil, a frame of reference such that x is parallel to the chord of the foil directed from the leading edge to the trailing edge, y is perpendicular to x and directed from the pressure side to the suction side, and the origin is located on the quarter-chord.

In this frame of reference, the pivot P has coordinates x_P, y_P. The flow generates a system of forces on the foil that can be decomposed into two in-plane forces and one moment normal to the plane, which are considered here to be applied at the quarter-chord of the foil.

The canonical decomposition is that of lift L and drag D, where lift is orthogonal to the free-stream reference velocity vector $\boldsymbol{u}_0$ and drag is parallel to it, and a moment M. The magnitudes of lift, drag, and moment are defined as

$$\hat{L} \equiv \frac{1}{2}\,\hat{\rho}\,\hat{u}^2\,\hat{c}\,C_L(\alpha), \tag{1}$$

$$\hat{D} \equiv \frac{1}{2}\,\hat{\rho}\,\hat{u}^2\,\hat{c}\,C_D(\alpha), \tag{2}$$

$$\hat{M} \equiv \frac{1}{2}\,\hat{\rho}\,\hat{u}^2\,\hat{c}^2\,C_M(\alpha), \tag{3}$$

27 January 2026 08:52:58

© Author(s) 2024

and the non-dimensional lift, drag, and moment are defined as

$$L = u^2\, C_L(\alpha), \tag{4}$$
$$D = u^2\, C_D(\alpha), \tag{5}$$
$$M = u^2\, C_M(\alpha), \tag{6}$$

which are assumed to be known and only a function of the foil geometry and the Reynolds number $Re_0 \equiv \hat{u}_0\hat{c}/\hat{\nu}$, where ν is the fluid kinematic viscosity. To simplify the notation used in the following equations, we also define the projections F_x and F_y of L and D on the foil-based frame of reference as

$$\begin{bmatrix} F_x \\ F_y \end{bmatrix} = u^2 \begin{bmatrix} C_x \\ C_y \end{bmatrix} = \begin{bmatrix} \cos(\alpha) & -\sin(\alpha) \\ \sin(\alpha) & \cos(\alpha) \end{bmatrix} \begin{bmatrix} D \\ L \end{bmatrix}. \tag{7}$$

Let us now assume that the foil is initially in equilibrium; that is, both the sum of forces and moments acting on the foil are equal to zero. This is always possible if, in addition to the aforementioned forces and moments, an additional torque $\hat{T}$ is applied to the foil to provide moment equilibrium about P, so that

$$\hat{F}_x(\alpha)\,\hat{y}_p - \hat{F}_y(\alpha)\,\hat{x}_p + \hat{M}(\alpha) + \hat{T} = 0. \tag{8}$$

This equation can be solved for all values of α and for any physical source of opposing torque $\hat{T}$. It was noted above that $\hat{T}$ can, for instance, be generated by musculoskeletal tension or by a torsional spring. Assume that $\hat{T}$ is an arbitrary function of the rotation of the foil in a fixed frame of reference, which we label β, and that

$$T(\beta) = \frac{\hat{T}(\beta)}{\frac{1}{2}\,\hat{\rho}\,\hat{u}_0^2\,\hat{c}^2}. \tag{9}$$

Let us denote the initial equilibrium condition with the subscript 0, so that the initial free-stream speed is $\hat{u}_0$, the initial angle of attack is α_0, and the initial angular position of the foil is β_0. Let us furthermore assume that the freestream velocity changes in magnitude and direction, so that the final absolute value is $\hat{u}_1$ and the angle with respect to the original location of the chord is $\alpha_0 + \alpha'$ (Fig. 1). The foil pitches around the pivot P to accommodate for the changes in inflow; as this is a solid rotation around P, the coordinates of P do not change in the foil frame of reference. At the new steady state, the new angle of attack is α_1, and the new forces and moments are $\hat{F}_x(\alpha_1)$, $\hat{F}_y(\alpha_1)$, and $\hat{M}(\alpha_1)$, respectively, while the opposing torque is $\hat{T}(\beta_1)$.

Note that $\alpha' \neq \alpha_1 - \alpha_0$, as $\alpha_1 - \alpha_0$ does not account for the extent of the rigid rotation of the foil. In fact, one has

$$\alpha_0 + \beta_0 + \alpha' = \alpha_1 + \beta_1. \tag{10}$$

All angles, forces, and moments, with the exception of T, are schematically represented in Fig. 1 for both the first steady state (in black) and the second steady state (in red).

As the foil is in equilibrium both before and after the gust, the balance of moments around P needs to be satisfied in both configurations. Analytically, this is represented by the following system:

$$\begin{cases} \hat{F}_x(\alpha_0)\,\hat{y}_p - \hat{F}_y(\alpha_0)\,\hat{x}_p + \hat{M}(\alpha_0) + \hat{T}(\beta_0) = 0, \\ \hat{F}_x(\alpha_1)\,\hat{y}_p - \hat{F}_y(\alpha_1)\,\hat{x}_p + \hat{M}(\alpha_1) + \hat{T}(\beta_1) = 0. \end{cases} \tag{11}$$

Nondimensionally, this system can be rewritten as

$$\begin{cases} C_x(\alpha_0)\,y_P - C_y(\alpha_0)\,x_P + C_M(\alpha_0) + T(\beta_0) = 0, \\ u_1^2(C_x(\alpha_1)\,y_P - C_y(\alpha_1)\,x_P + C_M(\alpha_1)) + T(\beta_1) = 0, \end{cases} \tag{12}$$

as $u_0 = 1$ by definition. Subtracting the two equations, one can reduce this system to

$$\begin{aligned} &C_x(\alpha_0)\,y_P - C_y(\alpha_0)\,x_P + C_M(\alpha_0) + T(\beta_0) \\ &\quad = u_1^2(C_x(\alpha_1)\,y_P - C_y(\alpha_1)\,x_P + C_M(\alpha_1)) + T(\beta_1). \end{aligned} \tag{13}$$

With prior knowledge of α_0, and if the position of the pivot (x_P, y_P) is known, then this equation can be solved to obtain the final angle of attack α_1. This equation is, however, non-linear in α_1 as the forces depend on C_L, C_D, and C_M, which are themselves not necessarily linear with α, and thus, the solution of Eq. (13) requires numerical root-finding.

Alternatively, the problem can be reframed as follows: given an initial state described by α_0, a gust described by α' and u_1, and a desired final angle of attack α_1, define the locus on which P needs to lie to satisfy this condition. With knowledge of α_1, then $C_x(\alpha_1)$, $C_y(\alpha_1)$, and $C_M(\alpha_1)$ are known by their definition, β_1 is known from Eq. (10), and the only unknowns are x_P and y_P. Equation (13) can thus be rewritten as

$$a_x\,x_P + a_y\,y_P + a_0 = 0, \tag{14}$$

where

$$a_x = -(C_y(\alpha_0) - u_1^2\,C_y(\alpha_1)), \tag{15a}$$
$$a_y = \ (C_x(\alpha_0) - u_1^2\,C_x(\alpha_1)), \tag{15b}$$
$$a_0 = -(C_M(\alpha_0) - u_1^2\,C_M(\alpha_1)) + T(\beta_1) - T(\beta_0). \tag{15c}$$

On this line, α_1 is constant by definition and β_1 is constant due to Eq. (10); therefore, all coefficients are constant with x_P and y_P, and this equation describes a straight line.

These results demonstrate that, for any arbitrary change in the onset flow speed and direction, pivots placed along the same line defined by Eq. (14) result in the same final angular position β_1 of the foil.

A. Minimum load change

By the inspection of the coefficients of lift, drag, and moment of a generic foil, it is trivial to show that, in general, there is no rotation or translation of the foil that would allow the same resultant force for both the initial and final flow velocity (see the Appendix for details). As the free-stream velocity changes, the foil passively rotates up to a position where the final moment equals the initial moment, but the initial and final resultant forces differ. We conclude that for a generic flow velocity fluctuation, a complete unsteady load mitigation is impossible by a passive rotation or translation.

However, we observe that for most natural flyers and engineering technologies, there is a direction along which it is more important to keep the force constant. For example, for a bird gliding near and parallel to the sea surface, maintaining a constant altitude and, therefore, upward force is critical, while accelerations in the direction parallel to the sea surface are not such a concern. We thus wonder whether

27 January 2026 08:52:58

© Author(s) 2024

complete mitigation of the load fluctuations in a selected direction is possible by a passive rotation or translation.

As described in the discussion following Eq. (15), Eq. (14) describes a line where both α_1 and β_1 are constant. As α_1 is constant, so are $C_x(\alpha_1)$ and $C_y(\alpha_1)$ as these only depend on α, and so are F_{x_1} and F_{y_1} following Eq. (7), and following that, the ratios F_{x_1}/F_{x_0} and F_{y_1}/F_{y_0} are also constant. This implies that for any generic direction $\boldsymbol{n}$ with respect to an earth-fixed frame, the ratio between the final and the initial force component F_{n_1}/F_{n_0} is also constant along the line. For example, consider a bird flying near the sea surface experiencing a streamwise gust. If the wings can passively pitch around a point P, the relative change of the force in the vertical direction depends only on the line on which P lies and not on the position of P along the line [Eq. (14)]. Furthermore, there is a line for which the latter relative change is zero, and thus, the force along the vertical direction remains constant.

As an example, Fig. 2 shows the lines of Eq. (14) for a set of forces computed with the coupled Euler-boundary layer solver XFOIL[42] for a NACA 0012 foil. The initial Reynolds number is $Re_0 \equiv u_0 c/\nu = 10^3$, where c is the chord length and ν is the kinematic viscosity of the fluid; the initial angle of attack is $\alpha_0 = 5°$; the torque T is constant; and the gust ratio is $u_1/u_0 = 2$. In this example, $\boldsymbol{n}$ is the lift direction. Here, we assume $\boldsymbol{u}_0$ to be the mean flow velocity, and $\boldsymbol{u}_1$ the perturbation, and thus, we define lift the force in the direction orthogonal to $\boldsymbol{u}_0$ also after the velocity has changed from $\boldsymbol{u}_0$ to $\boldsymbol{u}_1$. The colors show the ratio between the final and initial force along $\boldsymbol{n}$, i.e., the lift ratio L_1/L_0. Therefore, by passively pitching around an axis that intersects the line $L_1/L_0 = 1$ in Fig. 2, the lift remains constant despite the flow speed doubling.

These results reveal that the quasi-steady variations of an arbitrary chosen force component due to a gust ratio can be entirely canceled by passively pitching the foil around a specific pitching axis.

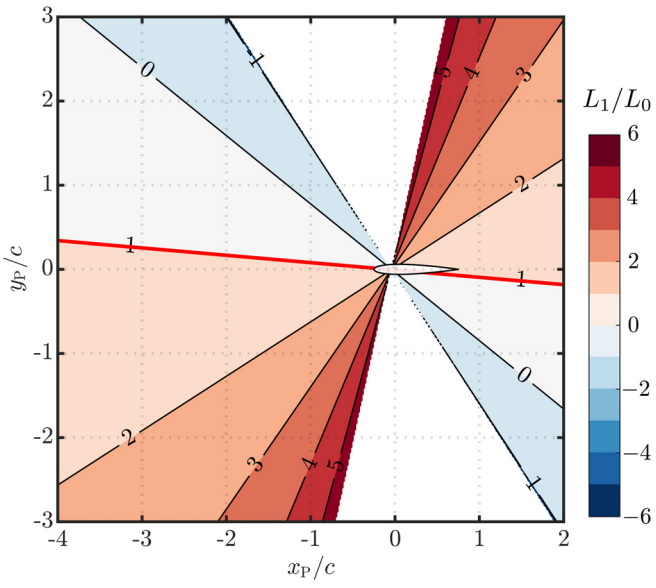

FIG. 2. Contours of lift ratio for different coordinates of the pitching axis of a NACA 0012 where the free-stream speed doubles ($u_1 = 2$) starting from $Re = 10^3$ at $\alpha_0 = 5°$. The solid red line shows the locus of the pitching axis for which the lift remains unchanged.

Note that an optimal center of rotation at $x_P < 0$ and $y_P \approx 0$ as suggested in Fig. 2, is equivalent to an upward and backward translation, and a nose-down rotation around the center of mass, which is consistent with the expected gust response of natural flyers.[27,30]

We now consider a free-stream velocity that varies in direction but not in magnitude. As we noted before, for a given flow speed, there is only one angle of incidence at which the fluid torque is in equilibrium with the externally applied constant torque T. Therefore, for any change α' of the angle of attack, the foil will rotate exactly by an angle α', resulting in the same initial and final resultant force vector with respect to a frame fixed with the foil. The projection of the resultant force vector $\boldsymbol{F}$ along any earth-fixed direction $\boldsymbol{n}$ would change by $\cos\alpha'$.

This reveals that, for a generic variation of the angle of attack, the force on the foil in a specific direction cannot be kept constant by a passive rotation or translation. However, for moderate angle of attack variations (α'), the force in any generic direction $\boldsymbol{n}$ changes only by a small amount (1-cos α'), which depends only on the amplitude of the angle of attack variation and not on, for example, the pitching axis location. For example, variations of 10° and 20° result in F_n changes of 1.5% and 6%, respectively.

Overall, these results reveal that (1) the fluctuations in an arbitrary chosen force component due to due to quasi-steady variations in flow speed can be entirely canceled by passive pitch; (2) the optimum pitching axis is at any arbitrary position along a line that depends only on the geometry of the foil [via its $C_l(\alpha)$, $C_d(\alpha)$, and $C_m(\alpha)$ curves], the initial and final Reynolds number; and (3) force fluctuations due to quasi-steady changes in the flow direction cannot be canceled, but substantial mitigation will be provided by pitching about any pitching axis.

B. Calculation of optimal pitching axis location

Given the previous findings, one can determine where to place the pitching axis with respect to the foil so as to keep one component of the force generated by the foil constant before and after a given gust.

To avoid overloading the notation, we assume that the arbitrary direction, along which we desire to keep the forces constant, is the same as that which has been used to define the angles β in Fig. 1; as this direction is arbitrary, this choice does not affect the generality of our conclusions.

We therefore define Q as the component of the force directed in the desired direction, which is related to the forces in the foil-fixed frame of reference by

$$\hat{Q} = \hat{F}_y(\alpha)\sin(\beta) - \hat{F}_x(\alpha)\cos(\beta). \tag{16}$$

Operating the same non-dimensionalization previously used, the equations that define the problem are the following:

$$\begin{aligned} &C_x(\alpha_0)\,y_P - C_y(\alpha_0)\,x_P + C_M(\alpha_0) + T(\beta_0) \\ &\quad = u_1^2(C_x(\alpha_1)\,y_P - C_y(\alpha_1)\,x_P + C_M(\alpha_1)) + T(\beta_1), \end{aligned} \tag{17a}$$

$$\begin{aligned} &C_y(\alpha_0)\sin(\beta_0) - C_x(\alpha_0)\cos(\beta_0) \\ &\quad = u_1^2(C_y(\alpha_1)\sin(\beta_1) - C_x(\alpha_1)\cos(\beta_1)), \end{aligned} \tag{17b}$$

$$\alpha_1 + \beta_1 = \alpha_0 + \beta_0 + \alpha'. \tag{17c}$$

In this system, Eq. (17a) represents the balance of moments previously presented as Eq. (13); Eq. (17b) states that $Q_1 = Q_0$; and

27 January 2026 08:52:58

© Author(s) 2024

Eq. (17c) is the geometric relationship between the angles involved previously presented as Eq. (10). One can see that the only dependence of the solution on P (x_P, y_P) is in Eq. (17a), and this system can be solved via substitution. Substituting

$$\beta_1 = (\alpha_0 + \beta_0 + \alpha') - \alpha_1 = \gamma_0 - \alpha_1 \tag{18}$$

in Eq. (17b), one has

$$C_y(\alpha_1)\sin(\gamma_0 - \alpha_1) - C_x(\alpha_1)\cos(\gamma_0 - \alpha_1) = \frac{C_y(\alpha_0)\sin(\beta_0) - C_x(\alpha_0)\cos(\beta_0)}{u_1^2}, \tag{19}$$

where $\gamma_0 = \alpha_0 + \beta_0 + \alpha'$ is known *a priori* and the only unknown in Eq. (19) is α_1. Equation (19) can then be solved numerically to yield the value of the angle of attack α_1 that satisfies the requirement of constant force component.

Once α_1 is found, this can be used in Eq. (14) and following to determine where the pivot should lie.

As all solutions of this system require that α_1 be constant, the set of values of (x_P, y_P) for which this is satisfied define an iso-line of α_1 in the $x_P - y_P$ space and therefore represent a straight line.

C. Stability of the equilibrium conditions

The previous analysis has only assumed that both the initial and the final steady state are equilibrium conditions, that is, they both individually satisfy the equalities in Eq. (12); no assumption on the stability of these solutions is made. For the foil at the initial steady state, equilibrium is given by Eq. (8); however, for non-equilibrium positions, one has to account for the angular acceleration of the foil so that in non-dimensional form,

$$J\ddot{\beta} = u^2(C_x(\alpha)\, y_P - C_y(\alpha)\, x_P + C_M(\alpha)) + T, \tag{20}$$

where J is the non-dimensional inertia of the foil,

$$J \equiv \frac{\hat{J}}{\frac{1}{2}\hat{\rho}\hat{c}^5}, \tag{21}$$

and $\hat{J}$ is the dimensional inertia.

Assume that a small perturbation changes the geometrical pitch of the foil so that it rotates around the pivot P increasing β by $d\beta$ and decreasing the angle of attack by $d\alpha = -d\beta$. The equilibrium position is stable if this induces a moment on the foil so that $\ddot{\beta} < 0$ to oppose $d\beta > 0$ and vice versa for $d\beta < 0$. Linearizing around the initial position, and, moreover, knowing that $d\beta = -d\alpha$, one has

$$J\ddot{\beta} = u^2\left(\frac{dC_x}{d\beta}\, y_P\, d\beta - \frac{dC_y}{d\beta}\, x_P\, d\beta + \frac{dC_M}{d\beta}\, d\beta\right) + \frac{dT}{d\beta}\, d\beta \tag{22}$$

$$= \left(u^2\left(-\frac{dC_x}{d\alpha}\, y_P + \frac{dC_y}{d\alpha}\, x_P - \frac{dC_M}{d\alpha}\right) + \frac{dT}{d\beta}\right) d\beta. \tag{23}$$

As J is positive by definition, one has a stable equilibrium if the term in parenthesis is less than zero, which is given by

$$u^2\left(\frac{dC_x}{d\alpha}\, y_P - \frac{dC_y}{d\alpha}\, x_P + \frac{dC_M}{d\alpha}\right) > -\frac{dT}{d\beta}, \tag{24}$$

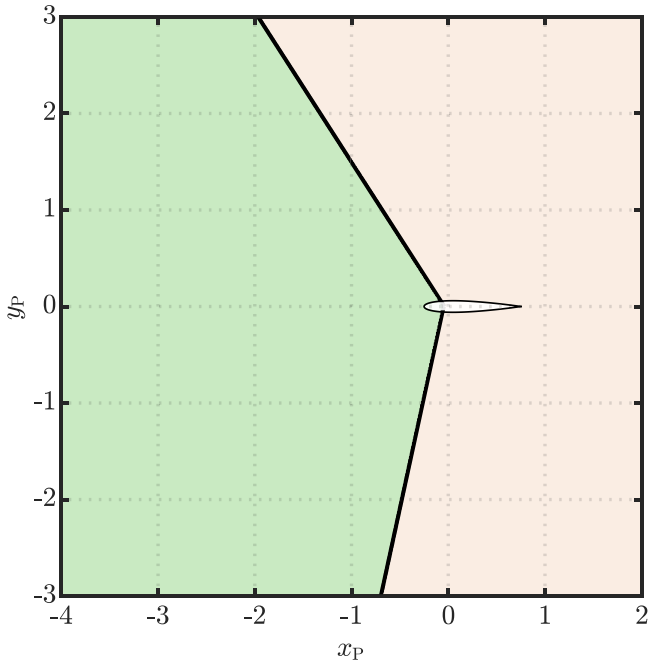

FIG. 3. Stable (green) and unstable (red) regions for the coordinates of the pivot P of a NACA 0012 where the free-stream speed doubles starting from $Re = 10^3$ at $\alpha_0 = 5°$.

which must be satisfied both at the initial and the final steady state. Note that, from Eq. (13), α_1 is only a function of u_1/u_0, x_P, and y_P: if the gust ratio is fixed, the coordinates of $P(x_P, y_P)$ for which the equilibrium is stable both before and after the gust can be readily found. For the case of a NACA 0012 foil, subject to a gust having $u_1 = 2$ and with initial $\alpha_0 = 5°$, one has the stability regions presented in Fig. 3 for a constant externally applied torque ($dT/d\beta = 0$). In this case, all stable pivot points are forward of the foil quarter-chord.

While in Fig. 2 we showed an example where T is constant, T can be any function of β (Sec. III). It is interesting to note that any pivot position results in stable equilibrium if $dT/d\beta$ is sufficiently small. Finally, it is noted that the modeled foil has only one degree of freedom in pitch, and thus, flutter is inhibited. Real wings, however, have multiple degrees of freedom and flutter instabilities might arise.

IV. UNSTEADY LOW-ORDER MODEL

To investigate the transient from the initial to the final equilibrium position, we employ a low-order model based on Kirchhoff's equations.[43] We consider the quasi-steady circulatory forces and added mass forces, but neglect the unsteady circulatory forces, which depend on the history of the flow field. This methodology has been validated against several experiments of free-falling bodies at $Re = 10^3$ to 10^4.[44–47]

Euler's second law of motion can be written for a frame of reference centered at the center of mass and with the x-axis along the chord, in vectorial notation, as

$$(I_O + I_M^A + m_{22}x_M^2)\dot{\boldsymbol{\omega}} = \boldsymbol{T} + \boldsymbol{M}^{QS} + \boldsymbol{x}_Q \times \boldsymbol{F}^{QS} - \boldsymbol{x}_P \times (\boldsymbol{F}^{QS} + \boldsymbol{F}^{AM}), \tag{25}$$

27 January 2026 08:52:58

© Author(s) 2024

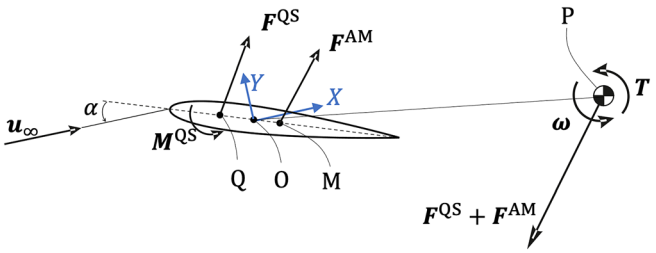

FIG. 4. Schematic diagram of the quasi-steady force (F^{QS}) acting at the quarter chord (Q) and the quasi-steady fluid moment (M^{QS}), the added mass force (F^{AM}) acting at the mid chord (M), the externally applied torque (T), and the angular velocity (ω) of the foil, all defined positive as in the figure. The figure also shows the reacting forces at the pivot P of the quasi-steady and added mass forces.

where I_O is the moment of inertia of the foil at the center of mass; I_Q^A is the added moment of inertia at the mid-chord (Fig. 4); this is translated to the center of mass through the parallel axis theorem through m_{22}, which is the second principal component of the added mass, and x_M is the coordinate of the mid-chord; $\dot{\omega}$ is the angular acceleration of the foil; $T = \kappa\beta$ is the externally applied torque, here considered proportional to the angular position of the foil β, with constant of proportionality κ; $\boldsymbol{M}^{QS}$ is the quasi-steady fluid moment when the quasi-steady force $\boldsymbol{F}^{QS}$ is applied at the quarter chord Q, whose position vector from the center of mass is $\boldsymbol{x}_Q$; $\boldsymbol{F}^{AM}$ is the added mass force applied at the mid chord M, whose position vector from the center of mass is $\boldsymbol{x}_M$; and finally, the last term is the torque due to the reacting forces $-\boldsymbol{F}^{QS} - \boldsymbol{F}^{AM}$ at the pivot point P with position vector $\boldsymbol{x}_P$. Because an analytical formulation for the added moment (I_A) and added mass force ($\boldsymbol{F}^{AM}$) is not available for a NACA foil, we consider those of an ellipse with the same chord and thickness[48] as described in Sec. IV A. The quasi-steady moment ($\boldsymbol{M}^{QS}$) and force ($\boldsymbol{F}^{QS}$) are computed from CFD simulations using the approach described in Sec. IV B. Equation (25) is solved in MATLAB with the `ode15i` function, which is a variable-step, variable-order solver based on the backward differentiation formulas of orders one to five.

A. Added-mass force

Figure 4 shows the vectors corresponding to the forces and moments considered in Eq. (25). The fluid force is modeled as the sum of the quasi-steady circulatory force $\boldsymbol{F}^{QS}$ applied at the quarter-chord point Q with position vector, $\boldsymbol{x}_Q$ from the center of mass O, and the added-mass force $\boldsymbol{F}^{AM}$ acting at the mid-chord M with position vector $\boldsymbol{x}_M$. The quasi-steady fluid moment is $\boldsymbol{M}^{QS}$, and the externally applied torque is $\boldsymbol{T}$. The foil's angular velocity is $\boldsymbol{\omega}$. Added mass forces are computed as follows.

The exact solution of the added moment of inertia, the second principal component of the added mass, and added-mass force on an ellipse[48] are, respectively,

$$I_Q^A = \frac{\pi}{128}\rho(c^2 - b^2)^2, \tag{26}$$

$$m_{22} = \frac{\pi\rho c^2}{4}, \tag{27}$$

$$F_x^{AM} = -\frac{\pi}{4}\rho c^2\left(\dot{\alpha}u_y + \frac{b^2}{c^2}\dot{u}_x\right), \tag{28}$$

$$F_y^{AM} = \frac{\pi}{4}\rho c^2\left(\frac{b^2}{c^2}\dot{\alpha}u_x - \dot{u}_y\right), \tag{29}$$

where b is the thickness (short axis); α is the angle of attack, and the dot denotes the time derivative (e.g., $\dot{\alpha} = d\alpha/dt$); and u_x and u_y are the chordwise and chord normal components of the relative velocity of the foil's mid-chord point M with respect to the free-stream velocity, such that $\boldsymbol{u} = (u_x, u_y) = \boldsymbol{u}_M - \boldsymbol{u}_\infty$.

B. Quasi-steady circulatory force

Apart from the added-mass force, the remainder of the lift, drag, and moment during the gust encounter are modeled in a quasi-steady manner based on tabulated CFD data. These data are generated by solving the two-dimensional Navier–Stokes equations for incompressible flows and Newtonian fluids with OpenFOAM v2106. The equations are solved in an inertial frame where the X and Y coordinates are parallel and orthogonal to $\boldsymbol{u}_0$, respectively. The computational domain consists of a rectangle $34c$ long (in the X direction) and $20c$ wide (in the Y direction), discretized by a structured grid (Fig. 5) generated using ICEM-CFD. Uniform velocity and pressure boundary conditions are Dirichlet conditions at the domain's upstream and downstream boundaries, respectively, while a slip condition is applied at the side boundaries.

Simulations are performed for $Re = 10^3$ and $Re = 2 \times 10^3$, for a range of angles of attack from 0° to 12°. The computed C_L^S, C_D^S, and C_M^S are shown in Fig. 6. Here, we set the Reynolds number of $\mathcal{O}(10^3)$ first because we are interested in the gust response of natural flyers (insects and small birds), nano air vehicles, and micro flyers. Second, $Re = 1000$ is sufficiently high to ensure the vorticity diffusion is negligible compared to advection, and sufficiently low to suppress lift fluctuations for a constant onset flow and angle of attack (e.g., due to wake instabilities and vortex shedding). For a higher Reynolds number, say $Re > \mathcal{O}(10^4)$, one can use XFOIL,[42] which provides sufficiently accurate prediction of forces.

These data are tabulated and interpolated at every time step to compute the quasi-steady forces and moment for the low-order model. Specifically, the quasi-steady circulatory lift, drag, and moment coefficients are computed as

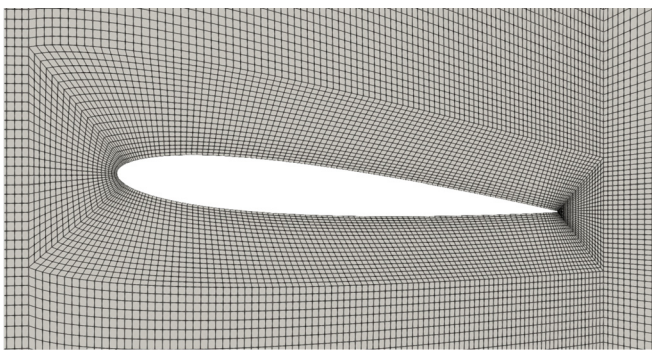

FIG. 5. Mesh of the CFD simulations used to compute the quasi-steady aerodynamic coefficients in Fig. 6.

27 January 2026 08:52:58

© Author(s) 2024

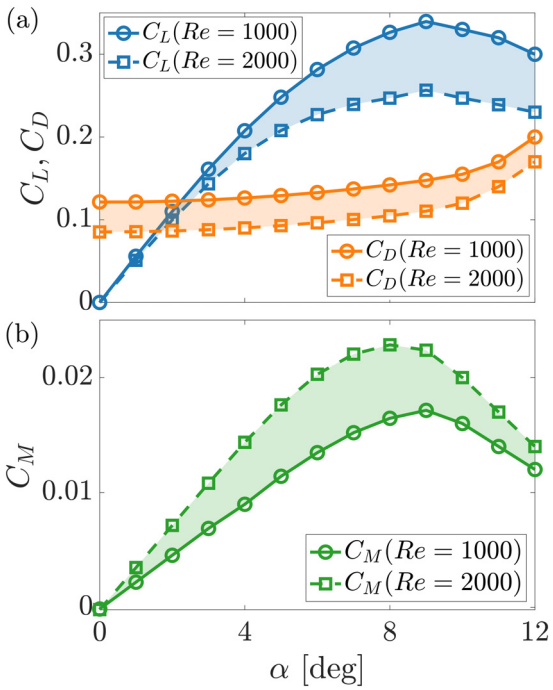

FIG. 6. Static lift and drag (a) and moment (b) coefficients vs angle of attack for $Re = 10^3$ and $Re = 2 \times 10^3$ obtained from CFD. Values within the shaded region are found by linear interpolation.

$$C_L^{QS} = C_L^S(\alpha_{eff}, Re)\left(\frac{u_X}{u_0}\right)^2,$$
$$C_D^{QS} = C_D^S(\alpha_{eff}, Re)\left(\frac{u_X}{u_0}\right)^2, \tag{30}$$
$$C_M^{QS} = C_M^S(\alpha_{eff}, Re)\left(\frac{u_X}{u_0}\right)^2,$$

where $u_X = u_\infty - u_{X,3qc}$ is the instantaneous streamwise velocity experienced by the foil; $u_{X,3qc}$ is the foil velocity in the streamwise X-axis direction (Fig. 4) at the three-quarter chord due to the passive pitching motion; and the effective angle of attack α_{eff} is the sum of the geometric angle of attack and the angle induced by the vertical motion of the foil,

$$\alpha_{eff} = \alpha - \arctan\left(\frac{u_{Y,3qc}}{u_{X,3qc}}\right), \tag{31}$$

where $u_{Y,3qc}$ is the foil velocity in the Y-direction at the three-quarter chord from the leading edge due to the passive pitch motion.

C. Gust profile

We consider a sharp change of the onset flow speed $u_\infty(t)$, which increases from u_0 to $2u_0$ in one convective time c/u_0 (Fig. 7). Specifically, the gust profile is given by

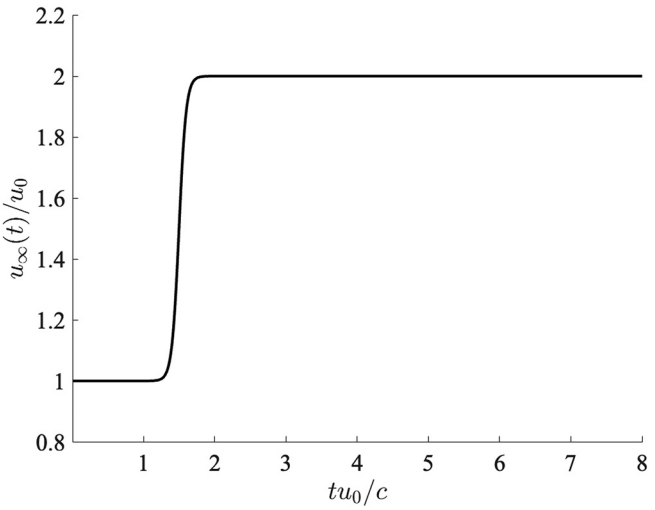

FIG. 7. Streamwise gust profiles.

$$u_\infty(t) = \begin{cases} u_0, & t \le \frac{c}{u_0}, \\ \frac{u_0}{2}(3 + \tanh\tau), & \frac{c}{u_0} < t < 2\frac{c}{u_0}, \\ 2u_0, & t \ge 2\frac{c}{u_0}, \end{cases} \tag{32}$$

where

$$\tau = \eta\left(\frac{tu_0}{c} - \frac{3}{2}\right), \tag{33}$$

and $\eta = 10$ is a gust sharpening factor.

It is important to note that this change in the flow speed occurs over a short time frame compared to the advection timescale of the flow, and the kinematics of the pitching foil would have changed marginally if the speed had increased over an even shorter time frame. In fact, as the gust period t_G over which the velocity changes from u_0 to $2u_0$ vanishes, the added mass force tends to infinity, while its duration tends to zero, and thus, the resultant added mass impulse would plateau to a finite value. The effect of the added mass is to generate vorticity (with net zero circulation) on the surface of the foil that is proportional to the added mass impulse. Hence, as $t_G \to 0$, the amount of added mass vorticity generated on the foil tends to a finite value. Therefore, the vorticity field at the start of the kinematics would not change significantly if $t_G \ll c/u_0$.

V. DYNAMIC ANALYSIS

The low order model described in Sec. IV is used to investigate the effect of the pitching axis location on the unsteady load mitigation, and specifically on the maximum amplitude of the lift fluctuation during the transient phase. Consider a change in the onset flow speed as detailed in Eq. (32). The initial condition is $\alpha_0 = 5°$, and the Reynolds number increases from $Re_0 = 10^3$ to $Re_1 = 2 \times 10^3$ in one convective time. The initial angle of attack $\alpha_0 = 5°$ is chosen because it is an intermediate angle between the zero-lift condition for a symmetric foil and the stall angle, which is typically of the order of 10°. The time history

27 January 2026 08:52:58

© Author(s) 2024

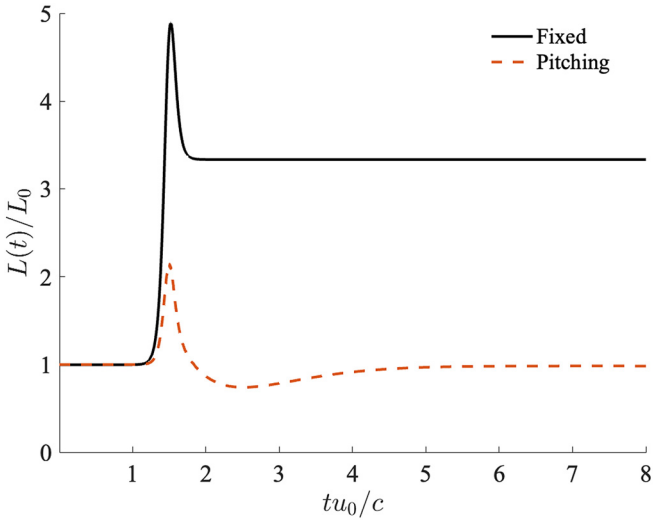

FIG. 8. Lift ratio vs non-dimensional time for a fixed and a passively pitching foil around a pivot at the foil-fixed coordinates $\boldsymbol{x}_P = (-1.5, 0.25)$.

of the lift $L(t)$ non-dimensionalized by the initial lift L_0 is shown in Fig. 8, for an example case with a pitching location at $\boldsymbol{x}_P = (-1.5, 0.25)$. The first sharp peak at $1 < tu_0/c < 2$ is due to added mass and, for the fixed foil, is proportional to the onset flow acceleration [i.e., the time derivative of Eq. (32)]. This first peak is substantially mitigated by the pitching foil, as it passively pitches in response to the load change. However, the pitching foil experiences a damped oscillation before reaching its final equilibrium position. Therefore, unlike for the fixed foil, the minimum lift is not necessarily the initial lift L_0: for some pitching locations, there is a lower minimum reached during the oscillation. In the example shown in Fig. 8, the minimum lift is achieved after the end of the gust at $t \approx 2c/u_0$.

A. Effect of pitching axis location on unsteady load mitigation

The model described in Sec. IV was used to investigate the effect of pitching axis location on the efficacy of unsteady load mitigation, within the stability constraints uncovered in Sec. III. We quantify the unsteady load mitigation as the ratio between the amplitude of the lift variations for the passively pitching foil and the fixed foil as

$$\varepsilon_{DY} = \frac{(C_{L,\max} - C_{L,\min})_{\text{pitch}}}{(C_{L,\max} - C_{L,\min})_{\text{fix}}}. \tag{34}$$

The load mitigation ratio ε_{DY} for the passively pitching foil experiencing increasing free-stream speed at a constant angle of 5° is shown in Fig. 9(a) for different pivot locations. Figure 9(b) shows the sensitivity of the ratio of dynamic lift fluctuation to the location of the pitching axes, $||\nabla\varepsilon_{DY}||$, under the same streamwise gust. $||\nabla\varepsilon_{DY}||$ is the modulus of $\nabla\varepsilon_{DY}$, where

$$\nabla\varepsilon_{DY} = (\partial\varepsilon_{DY}/\partial X_P, \partial\varepsilon_{DY}\partial Y_P). \tag{35}$$

The sensitivity increases with increasing X_P and Y_P [Fig. 9(b)], where the stability analysis (Sec. III C) showed an unstable region.

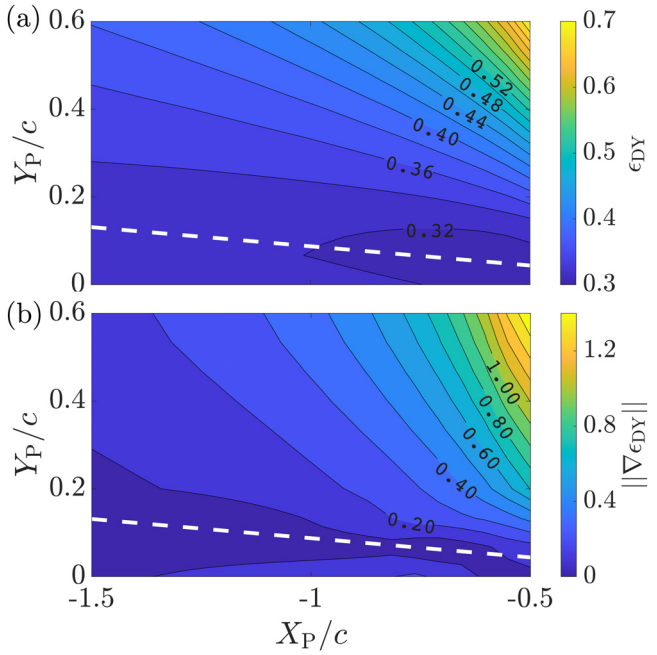

FIG. 9. Contours of the dynamic unsteady load mitigation index (a) and of its spatial gradient (b) for different coordinates of the pitching axis location. The dashed line shows the extended chord line.

The map of ε_{DY} (Fig. 9) suggests that the maximum unsteady load alleviation is achieved for a pitching axis located along the extended chord line (indicated with a white dotted line in Fig. 9). This is consistent with the results shown for a quasi-steady analysis in Fig. 2. Furthermore, the sensitivity of ε_{DY} to the exact location decreases as the pitching axis approaches the extended chord line. Hence, these results suggest that the optimum location of the pitching axis is along the extended chord line. While the quasi-steady analysis showed that the unsteady load alleviation depends on the line on which the pitching axis lies and not on its distance from the foil (see Fig. 2), the dynamic analysis, in contrast, suggests that the position along the extended chord line is important. We will discuss the optimal position along the extended chord line in Sec. V B.

To further understand the underlying physics resulting in the optimum pitching axis, we study the effect of pitching axis on the maximum and minimum lift peaks separately. The maximum lift $C_{L\max}$ is only marginally affected by pitching axis location [Fig. 10(a)], and the maximum alleviation of $C_{L\max}$ is achieved with a pitching axis at approximately $\boldsymbol{X}_P = (-1, 0.5)$. On the other hand, the minimum lift $C_{L\min}$, which is due to the oscillations of the foil as it approaches the new equilibrium position, is highly dependent on the pitching axis location [Fig. 10(a)], and thus, the optimum pitching position is governed by $C_{L\min}$ [cf. Figs. 9(a) and 10(b)]. Specifically, the maximum alleviation of the negative lift peak is achieved for pitching axes along the extended chord line of the foil. Moreover, similarly to ε_{DY}, $C_{L\min}$ decreases with increasing X/c.

We further dissect the contribution of the added mass and quasi-steady lifts to the maximum and minimum lift. While the position of the pitching axis minimizing the positive lift peak $C_{L\max}$ is

27 January 2026 08:52:58

© Author(s) 2024

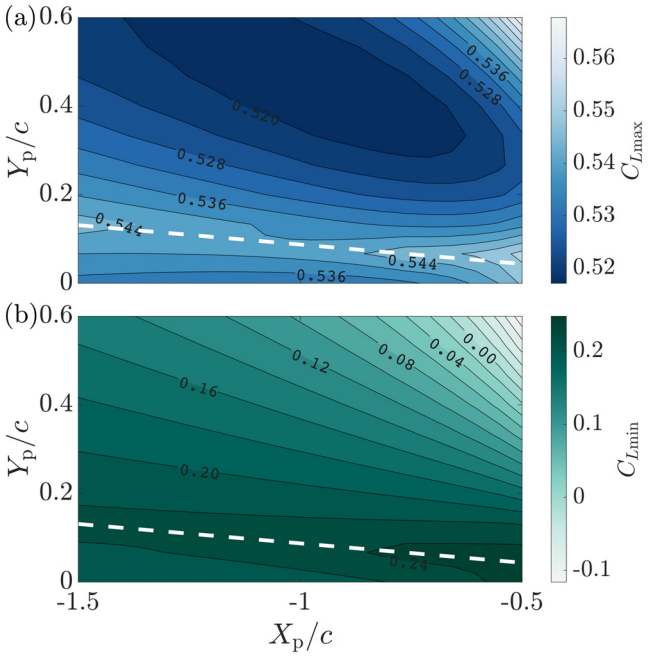

FIG. 10. Contours of the maximum (a) and minimum (b) value of the lift coefficient for different coordinates of the pitching axis location. The dashed line shows the extended chord line.

approximately at $\boldsymbol{X}_P = (-1, 0.5)$, the pitching axis would need to be further away from the foil to minimize the sole added mass lift peak, and closer to the foil to minimize the quasi-steady lift peak [Figs. 11(a) and 11(b)]. This result reveals that the optimal distance of the pitching axis to mitigate the maximum lift is a compromise between added mass and quasi-steady force, even if the maximum lift plays a minor part in the overall lift fluctuation, which, instead, is governed by the minimum lift. Conversely, placing the pitching axis along the extended chord line contributes to increasing both the minimum lift due to added mass and quasi-steady force [Figs. 11(c) and 11(d)].

B. Pitching axis on the extended chord line

To understand what determines the optimal distance of the pitching axis and the balance between added mass and quasi-steady forces, we consider the pitching axis on the extended chord line (i.e., on the white dotted line in Fig. 9), and we plot the trend of ε_{DY} vs the X coordinates of the pitching axis (Fig. 12). We observe that ε_{DY} is minimum at $X/c = -0.83$, which is also where the maximum lift has the lowest value [Fig. 12(b)]. Around $X_p/c = -0.73$, C_{Lmin} increases with decreasing distance from the foil, and at $X_p/c = -0.73$, it has the same value as the initial lift value, $C_{L0} = 0.248$ [Fig. 12(c)].

We will show now that this optimum pitching axis coordinate, $X_p/c = -0.73$, depends on the inertia of the system. For an increased distance of the pitching axis from the foil, the inertia increases, and the overshoot generating the minimum lift decreases [Fig. 12(c)]. Therefore, ε_{DY} initially decreases with the distance of the pitching axis from the foil. However, for a further increased inertia, the foil is slow to accelerate at the beginning of the gust, and thus, the maximum lift

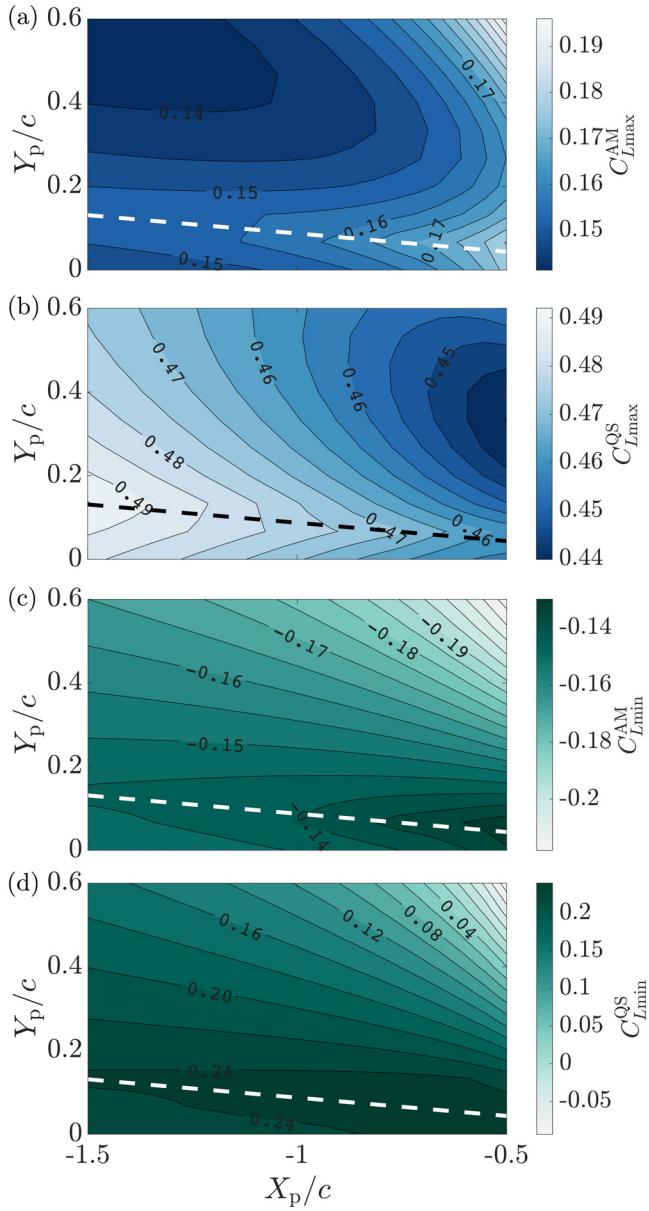

FIG. 11. Contours of the maximum (a) and (b) and minimum (c) and (d) value of the lift coefficient due to the added mass (a) and (c) and quasi-steady force (b) and (d) for different coordinates of the pitching axis location. The dashed line shows the extended chord line.

increases [Fig. 12(b)]. Therefore, there is an optimal system inertia such that the minimum lift peak due to the overshoot is not lower than the initial lift. Specifically, the higher the inertia, the closer the optimal pitching axis will be to the wing.

To demonstrate this, we consider the time history of lift C_L for three selected cases [identified as case 1, 2, and 3 in Fig. 12(a)]. Case 1 has the pitching axis at $X_p/c = -0.5$, case 2 at $X_p/c = -0.73$ (the optimal pitching axis location), and case 3 at $X_p/c = -722$. In case 1

27 January 2026 08:52:58

© Author(s) 2024

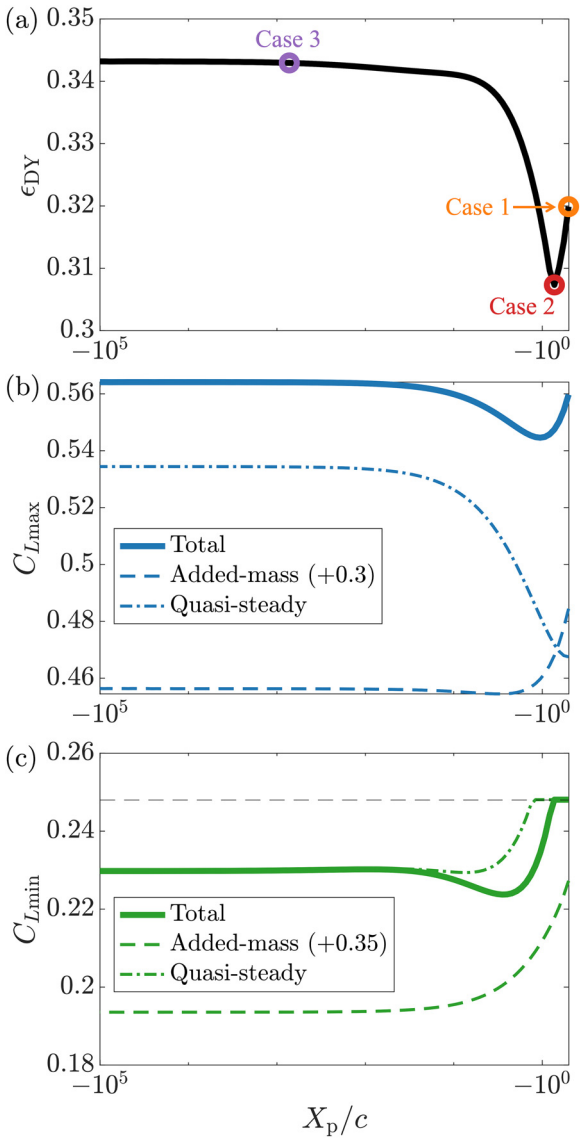

FIG. 12. Unsteady load mitigation index (a), maximum lift (b), and minimum lift (c) for pitching axis on the extended chord line and different streamwise coordinates. For better visibility of the trends, 0.3 and 0.35 are added to the maximum and minimum added-mass lift coefficients, respectively. Three cases (case 1, case 2, and case 3) are marked for the following analysis.

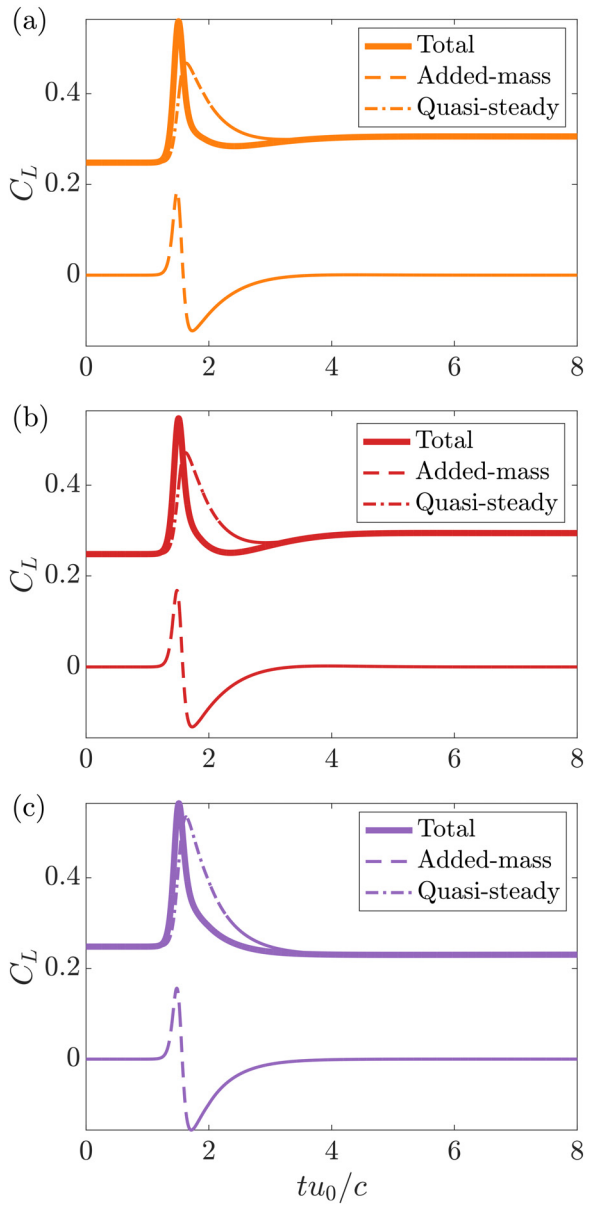

FIG. 13. Time history of the lift coefficient and its contributions due to added mass and quasi-steady force for case 1 (a), case 2 (b), and case 3 (c).

[Fig. 13(a)], the minimum lift is the initial lift, $C_{Lmin} = C_{L0}$ and the lift after the peak is always higher than C_{L0}. In case 2 [Fig. 13(b)], which is the maximum lift alleviation case, the lift after the peak becomes as low as the initial lift at $tu_0/c \approx 2$. Finally, in case 3 [Fig. 13(c)], the lift after the peak is smaller than the initial lift C_{L0}. These results explain why the minimum ε_{DY} is minimum for the same X_p for which $C_{L,max}$ is minimum, even if before (Fig. 10) we concluded that the optimum pitching axis location is governed by $C_{L,min}$ and not $C_{L,max}$.

The kinematics of the three cases (Fig. 14) reveal the underlying physics for the time series of the lift observed in Fig. 13. The angle of attack decreases in response to the change in the free-stream speed to reach the new equilibrium position [Fig. 13(a)]. The higher the inertia, the lower the magnitude of the rate of change of the angle of attack [Fig. 13(b)]. Consistently, the acceleration of the angle of attack shows a negative peak corresponding to the foil angular velocity becoming negative, and a positive peak corresponding to the vanishing angular velocity as the foil approaches the new equilibrium position.

Noting that $b \ll c$, the dominant added mass force component is proportional to the acceleration $\dot{u}_y$ [Eq. (29)], which is correlated with the acceleration of the angle of attack through $r_{mc}\ddot{\alpha} = \dot{u}_x^2 + \dot{u}_y^2$, where

27 January 2026 08:52:58

© Author(s) 2024

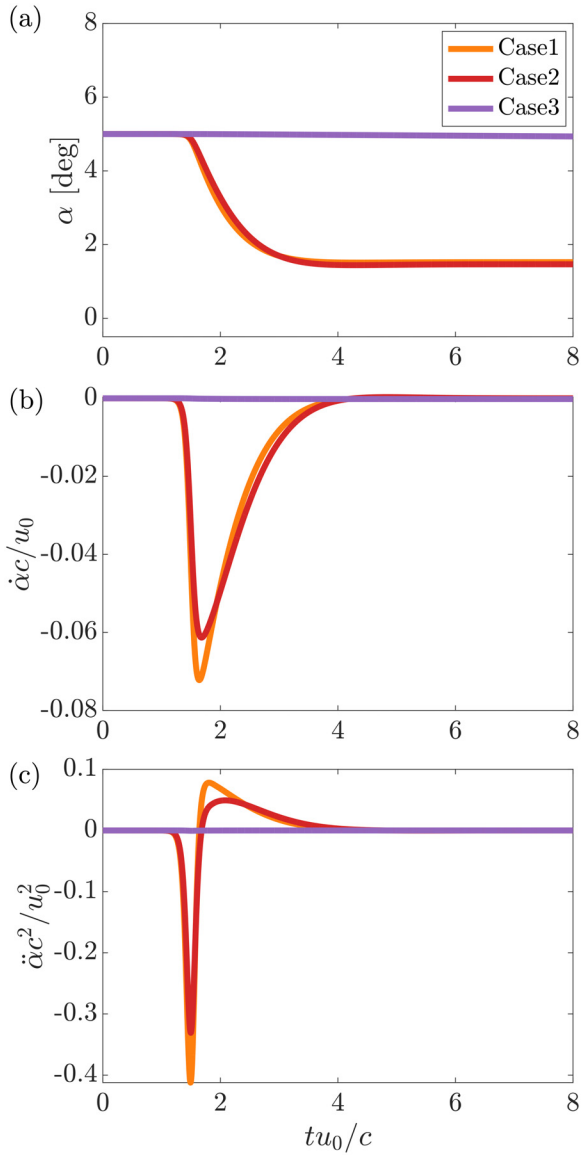

FIG. 14. Time history of the angle of attack, and thus of the angular position of the foil (a), and of its nondimensional first (b) and second (c) time derivatives.

r_{mc} is the distance between the pivot and the center of mass (|PO|). For a pitching axis along the extended chord line and small initial angle of attack, the rotation along the pivot corresponds to a chord normal velocity, i.e., $r_{mc}\ddot{\alpha} \approx \dot{u}_y^2$. The velocity $r_{mc}\dot{\alpha}$ and the acceleration $r_{mc}\ddot{\alpha}$ are shown in nondimensional form in Fig. 15. As one would expect, the higher the inertia (from cases 1 to 3), the later the maximum velocity is reached [Fig. 15(a)] and the slower the velocity decreases after the peak. Therefore, while the positive acceleration peak increases with inertia (case 3), the magnitude of the deceleration peak decreases with inertia. These results reveal why the maximum added mass lift peak is better mitigated by pitching axes far from the

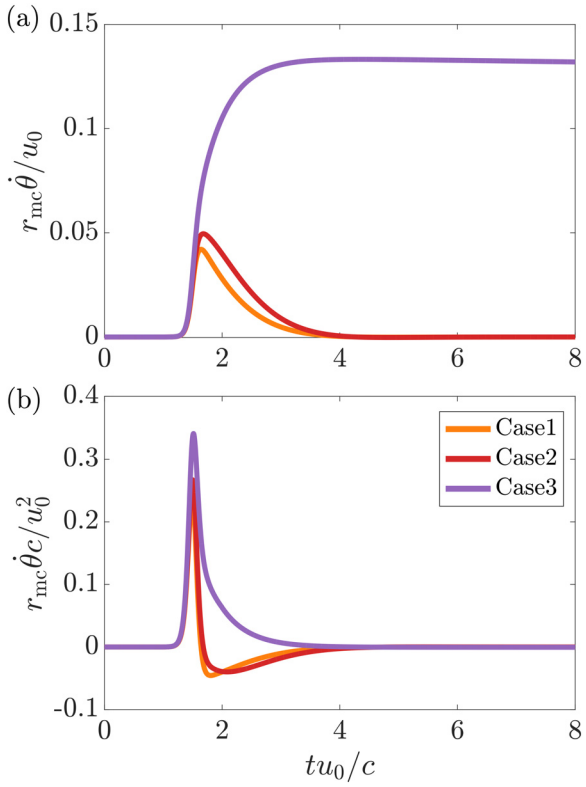

FIG. 15. Time history of the nondimensional tangential velocity (a) and acceleration (b) of the foil.

foil [Fig. 11(a)], while the minimum added mass lift peak is better mitigated by pitching axes closer to the foil [Fig. 11(c)].

The quasi-steady force, instead, depends on the effective angle of attack α_{eff} [Fig. 16(a)], which is the angle between the chord and the relative velocity experienced by the foil $\boldsymbol{u}_\infty + \boldsymbol{u}_M$. The time histories of α_{eff} are similar for the three cases [Fig. 16(a)]. However, when these are scaled with the square of the instantaneous free-stream velocity [Fig. 16(b)], the amplitude of both the maximum and the minimum peak increases with increasing inertia. This reveals why both the maximum [Fig. 11(b)] and minimum [Fig. 11(d)] quasi-steady lift are better mitigated by pitching closer to the foil.

VI. CONCLUSIONS

In this paper, a general approach for the design of efficient passive pitch systems has been developed. Their capabilities and limitations in mitigating unsteady loads have been investigated. We considered a foil in a uniform free stream, which is free to rotate around a pitching axis and is held in position by an externally applied torque. The system is passive because the applied torque is either constant or varies linearly with the angular position of the foil. Such a system can be achieved, for example, by a linear torsional spring. We developed a mathematical framework to compute how a generic force component varies when the onset flow velocity changes, in a quasi-steady manner, to a new uniform speed and direction. We showed that any force component can be kept constant if the locus of the pivot is a line that depends on

27 January 2026 08:52:58

© Author(s) 2024

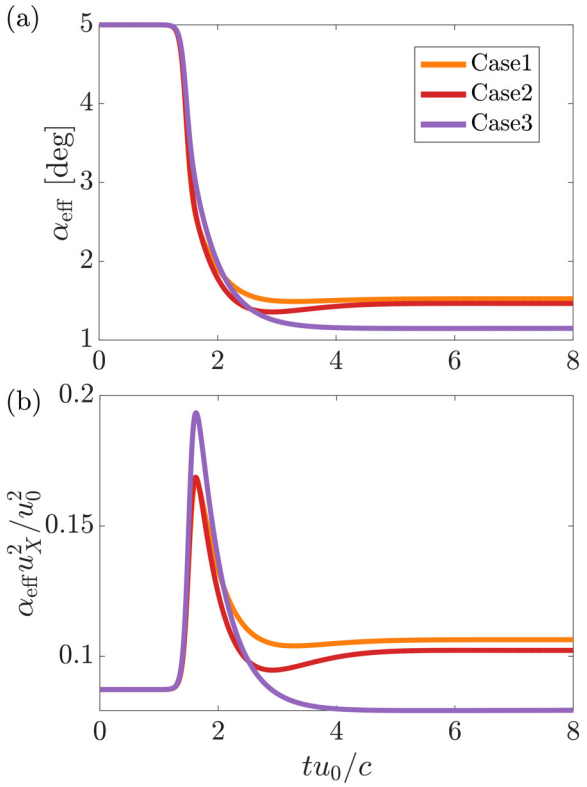

FIG. 16. Time history of the effective angle of attack (a) and of the effective angle of attack scaled with the instantaneous free-stream speed (b).

the initial and final flow velocity and the aerodynamic polars (lift, drag, and moment coefficients) of the foil.

Furthermore, we developed a dynamic model that includes analytical formulations of the added mass forces and tabulated quasi-steady aerodynamic polars. The model enables estimation of the dynamic response of the foil in the transient between the initial and final equilibrium state. We applied the model for the lift generated by a foil at a small angle of incidence (5°), experiencing a rapid twofold increase in freestream velocity. More than 2/3 of the lift fluctuation can be canceled by placing the pivot point along the extended chord line at a distance from the foil that increases with decreasing inertia. The foil first experiences a lift increase and thus pitches reducing the angle of incidence, and then, it oscillates until it reaches the final equilibrium position. The optimum pivot position is such that the minimum lift during the transient is equal to the initial lift. While the optimal positioning of the pitching axis may vary with gust parameters, the efficacy of load mitigation shows minimal sensitivity to the precise location within the vicinity of the optimal locus.

The present study focuses on the passive pitch system at relatively low Reynolds numbers, $Re = \mathcal{O}(10^3)$, but yet the pressure forces dominate the viscous forces. As long as this remains true, such as at higher Reynolds numbers, the present results are expected to stand. For situations where the viscous forces dominate, such as very low Reynolds numbers or non-Newtonian flows, the results should be reviewed.

In the present work, the pivot point is fixed during the transient. Therefore, this work may potentially underestimate the efficacy of advanced systems such as adjustable musculoskeletal tension, dynamic pitching axes or joints, and temporary modifications in foil positioning through dihedral angle adjustments, among others. Additionally, the passive mechanism examined here is inadequate for handling stall conditions, which necessitate active stabilization methods.

Overall, this work provides a new methodology for studying different gust types and designing optimal passive pitch systems. It also provides new insights into the underlying physics of gust mitigation through passive pitching. As such, it may also enrich our understanding of complex biological passive systems observed in nature.

ACKNOWLEDGMENTS

This work was supported by the UK Engineering and Physical Sciences Research Council through the grant "Morphing-Blades: New-Concept Turbine Blades for Unsteady Load Mitigation" (No. EP/V009443/1).

AUTHOR DECLARATIONS

Conflict of Interest

The authors have no conflicts to disclose.

Author Contributions

Shūji Ōtomo: Conceptualization (lead); Data curation (lead); Formal analysis (lead); Investigation (lead); Methodology (lead); Software (lead); Visualization (lead); Writing – original draft (lead). **Stefano Gambuzza:** Conceptualization (lead); Data curation (lead); Formal analysis (lead); Investigation (lead); Methodology (lead); Software (lead); Visualization (lead); Writing – original draft (lead). **Yabin Liu:** Data curation (equal); Formal analysis (equal); Investigation (equal); Methodology (equal); Software (equal); Validation (equal); Visualization (equal); Writing – review & editing (equal). **Anna M. Young:** Funding acquisition (equal); Supervision (equal); Writing – review & editing (equal). **Riccardo Broglia:** Funding acquisition (supporting); Supervision (equal); Writing – review & editing (equal). **Edward D. McCarthy:** Funding acquisition (equal); Supervision (equal); Writing – review & editing (equal). **Ignazio Maria Viola:** Conceptualization (lead); Formal analysis (lead); Funding acquisition (lead); Methodology (lead); Project administration (lead); Resources (lead); Supervision (lead); Writing – original draft (lead).

DATA AVAILABILITY

The data that support the findings of this study are available from the corresponding author upon reasonable request.

APPENDIX: UNIQUENESS OF *L* AND *D* FOR EACH *A*

The forces generated by a foil exposed to an incoming flow are customarily decomposed in a component normal to the incoming velocity, i.e., the lift L, and one parallel to it, i.e., the drag D. In non-dimensional form, these are the lift C_L and drag C_D coefficients,

$$C_L \equiv \frac{L}{\frac{1}{2}\rho u_\infty^2 c}, \tag{A1}$$

27 January 2026 08:52:58

© Author(s) 2024

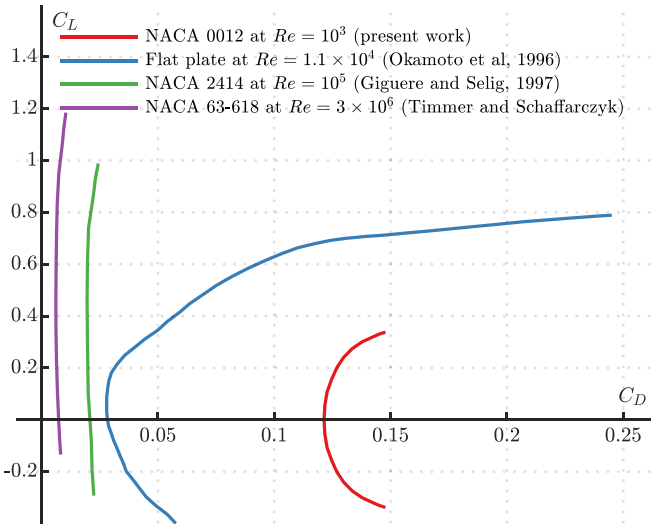

FIG. 17. Polar curves of selected foils at a range of Reynolds number values, including data from Okamoto *et al.*,[49] Giguère and Selig,[50] and Timmer and Schaffarczyk.[51]

$$C_D \equiv \frac{D}{\frac{1}{2}\rho u_\infty^2 c}. \tag{A2}$$

These coefficients are functions of the chord-based Reynolds number Re,

$$Re \equiv \frac{u_\infty c}{\nu}. \tag{A3}$$

For a generic foil shape generating a lift and drag coefficient C_L and C_D, respectively, at a given value of Re and angle of attack α, there is at most one value of α for which that lift and drag are attained. This can be graphically observed by plotting the parametric curve,

$$\begin{cases} C_L = C_L(\alpha), \\ C_D = C_D(\alpha), \end{cases} \tag{A4}$$

on the $C_L - C_D$ space and observing that this curve does not self-intersect.

Figure 17 reports the polars for four different foils at four different values of chord-based Reynolds number Re, spanning from 10^3 to 10^6. These are the NACA 0012 presented in this work; a flat plate operating at $Re = 1.1 \times 10^4$ representative of a dragonfly wing;[49] a NACA 2414 operating at $Re = 10^5$ representative of a small horizontal-axis wind turbine;[50] and a NACA 63-618 for use in larger-scale wind turbines.[51] The NACA 0012 data are computed with direct numerical simulations, while all other polars come from experimental measurements in wind tunnels. It can be seen that the polar curves do not self-intersect in any case, demonstrating that, in general, there is at most one value of α for each pair of C_L and C_D.

REFERENCES

[1]L. Paull, S. Saeedi, M. Seto, and H. Li, "AUV navigation and localization: A review," IEEE J. Oceanic Eng. **39**, 131–149 (2014).
[2]A. Aguiar and A. Pascoal, "Dynamic positioning and way-point tracking of underactuated AUVs in the presence of ocean currents," Int. J. Control **80**, 1092–1108 (2007).
[3]J. J. Leonard and A. Bahr, "Autonomous underwater vehicle navigation," in *Springer Handbook of Ocean Engineering* (Springer, 2016), pp. 341–357.
[4]N. E. Leonard and J. G. Graver, "Model-based feedback control of autonomous underwater gliders," IEEE J. Oceanic Eng. **26**, 633–645 (2001).
[5]J. M. Anderson and N. K. Chhabra, "Maneuvering and stability performance of a robotic tuna," Integr. Comp. Biol. **42**, 118–126 (2002).
[6]A. Seifert, D. Greenblatt, and I. J. Wygnanski, "Active separation control: An overview of Reynolds and Mach numbers effects," Aerosp. Sci. Technol. **8**, 569–582 (2004).
[7]E. Stanewsky, "Adaptive wing and flow control technology," Prog. Aerosp. Sci. **37**, 583–667 (2001).
[8]L. N. Cattafesta III and M. Sheplak, "Actuators for active flow control," Annu. Rev. Fluid Mech. **43**, 247–272 (2011).
[9]I. K. Kuder, A. F. Arrieta, W. E. Raither, and P. Ermanni, "Progress in aerospace sciences variable stiffness material and structural concepts for morphing applications," Prog. Aerosp. Sci. **63**, 33–55 (2013).
[10]F. Afonso, J. Vale, É. Oliveira, F. Lau, and A. Suleman, "A review on non-linear aeroelasticity of high aspect-ratio wings," Prog. Aerosp. Sci. **89**, 40–57 (2017).
[11]D. Li, S. Zhao, A. Da Ronch, J. Xiang, J. Drofelnik, Y. Li, L. Zhang, Y. Wu, M. Kintscher, H. P. Monner, A. Rudenko, S. Guo, W. Yin, J. Kirn, S. Storm, and R. D. Breuker, "A review of modelling and analysis of morphing wings," Prog. Aerosp. Sci. **100**, 46–62 (2018).
[12]T. K. Barlas and G. A. M. van Kuik, "Review of state of the art in smart rotor control research for wind turbines," Prog. Aerosp. Sci. **46**, 1–27 (2010).
[13]P. B. Andersen, Ph.D. thesis, Technical University of Denmark, 2005.
[14]D. W. MacPhee and A. Beyene, "Experimental and fluid structure interaction analysis of a morphing wind turbine rotor," Energy **90**, 1055–1065 (2015).
[15]D. Floreano and R. J. Wood, "Science, technology and the future of small autonomous drones," Nature **521**, 460–466 (2015).
[16]S. Watkins, J. Milbank, B. J. Loxton, and W. H. Melbourne, "Atmospheric winds and their implications for microair vehicles," AIAA J. **44**, 2591–2600 (2006).
[17]M. Kambushev, S. Biliderov, K. Yovchev, D. Chikurtev, K. Kambushev, and N. Chivarov, "Influence of atmospheric turbulence on the control of flying robotics systems," in *IEEE XXVIII International Scientific Conference Electronics (ET)* (IEEE, 2019).
[18]D. E. Findeis, M. G. Balchanos, G. Vachtsevanos, and D. N. Mavris, "Modeling and simulation of uav swarm formation control in response to wind gusts," AIAA Paper No. 2019-1571, 2019.
[19]M. Di Luca, S. Mintchev, Y. Su, E. Shaw, and K. Breuer, "A bioinspired separated flow wing provides turbulence resilience and aerodynamic efficiency for miniature drones," Sci. Rob. **5**, eaay8533 (2020).
[20]A. R. Jones, O. Cetiner, and M. J. Smith, "Physics and modeling of large flow disturbances: Discrete gust encounters for modern air vehicles," Annu. Rev. Fluid Mech. **54**, 469–493 (2022).
[21]M. A. Lackner and G. van Kuik, "A comparison of smart rotor control approaches using trailing edge flaps and individual pitch control," Wind Energy **13**, 117–134 (2010).
[22]V. Cognet, S. Courrech Du Pont, I. Dobrev, F. Massouh, and B. Thiria, "Bioinspired turbine blades offer new perspectives for wind energy," Proc. R. Soc. A **473**, 20160726 (2017).
[23]I. M. Viola, G. Pisetta, W. Dai, A. Arredondo-Galeana, A. Young, and A. Smyth, "Morphing blades: Theory and proof of principles," Int. J. Mar. Energy **5**, 183–193 (2022).
[24]W. Dai, R. Broglia, and I. M. Viola, "Mitigation of rotor thrust fluctuations through passive pitch," J. Fluids Struct. **112**, 103599 (2022).
[25]G. Pisetta, R. Le Mestre, and I. M. Viola, "Morphing blades for tidal turbines: A theoretical study," Renewable Energy **183**, 802–819 (2022).
[26]K. Nishikawa, A. A. Biewener, P. Aerts, A. N. Ahn, H. J. Chiel, M. A. Daley, T. L. Daniel, R. J. Full, M. E. Hale, T. L. Hedrick *et al.*, "Neuromechanics: An integrative approach for understanding motor control," Integr. Comp. Biol. **47**, 16–54 (2007).
[27]C. Harvey, V. Baliga, P. Lavoie, and D. Altshuler, "Wing morphing allows gulls to modulate static pitch stability during gliding," J. R. Soc. Interface **16**, 20180641 (2019).

27 January 2026 08:52:58

© Author(s) 2024

[28]C. Harvey, V. Baliga, J. Wong, D. Altshuler, and D. Inman, "Birds can transition between stable and unstable states via wing morphing," Nature **603**, 648–653 (2022).
[29]A. J. Bergou, L. Ristroph, J. Guckenheimer, I. Cohen, and Z. J. Wang, "Fruit flies modulate passive wing pitching to generate in-flight turns," Phys. Rev. Lett. **104**, 148101 (2010).
[30]J. Vance, I. Faruque, and J. Humbert, "Kinematic strategies for mitigating gust perturbations in insects," Bioinspiration Biomimetics **8**, 016004 (2013).
[31]E. A. Mistick, A. M. Mountcastle, and S. A. Combes, "Wing flexibility improves bumblebee flight stability," J. Exp. Biol. **219**, 3384–3390 (2016).
[32]J. Videler, D. Weihs, and S. Daan, "Intermittent gliding in the hunting flight of the kestrel, *Falco tinnunculus* L," J. Exp. Biol **102**, 1–12 (1983).
[33]J. Videler and A. Groenewold, "Field measurements of hanging flight aerodynamics in the kestrel *Falco tinnunculus*," J. Exp. Biol. **155**, 519–530 (1991).
[34]R. A. Meyers, "Morphology of the shoulder musculature of the American kestrel, *Falco sparverius* (Aves), with implications for gliding flight," Zoomorphology **112**, 91–103 (1992).
[35]A. Fisher, M. Marino, R. Clothier, S. Watkins, L. Peters, and J. L. Palmer, "Emulating avian orographic soaring with a small autonomous glider," Bioinspiration Biomimetics **11**, 016002 (2015).
[36]J. A. Cheney, J. P. Stevenson, N. E. Durston, J. Song, J. R. Usherwood, R. J. Bomphrey, and S. P. Windsor, "Bird wings act as a suspension system that rejects gusts," Proc. R. Soc. B **287**, 20201748 (2020).
[37]J. A. Cheney, N. Konow, K. M. Middleton, K. S. Breuer, T. J. Roberts, E. L. Giblin, and S. M. Swartz, "Membrane muscle function in the compliant wings of bats," Bioinspiration Biomimetics **9**, 025007 (2014).
[38]C. Harvey and D. J. Inman, "Gull dynamic pitch stability is controlled by wing morphing," Proc. Natl. Acad. Sci. U. S. A. **119**, e2204847119 (2022).
[39]S. Ravi, D. Kolomenskiy, T. Engels, K. Schneider, C. Wang, J. Sesterhenn, and H. Liu, "Bumblebees minimize control challenges by combining active and passive modes in unsteady winds," Sci. Rep. **6**, 35043 (2016).
[40]R. Dakin, P. S. Segre, A. D. Straw, and D. L. Altshuler, "Morphology, muscle capacity, skill, and maneuvering ability in hummingbirds," Science **359**, 653–657 (2018).
[41]S. Gambuzza, G. Pisetta, T. Davey, J. Steynor, and I. M. Viola, "Model-scale experiments of passive pitch control for tidal turbines," Renewable Energy **205**, 10–29 (2023).
[42]M. Drela, "Xfoil: An analysis and design system for low reynolds number airfoils," in *Low Reynolds Number Aerodynamics* (Springer, 1989).
[43]H. Lamb *et al.*, *Hydrodynamics* (Dover, New York, 1945), available at https://archive.org/details/hydrodynamics00lamb.
[44]A. Andersen, U. Pesavento, and Z. J. Wang, "Unsteady aerodynamics of fluttering and tumbling plates," J. Fluid Mech. **541**, 65 (2005).
[45]A. Andersen, U. Pesavento, and Z. J. Wang, "Analysis of transitions between fluttering, tumbling and steady descent of falling cards," J. Fluid Mech. **541**, 91–104 (2005).
[46]W. Huang, H. Liu, F. Wang, J. Wu, and H. P. Zhang, "Experimetal study of a freely falling plate with an inhomogeneous mass distribution," Phys. Rev. E **88**, 053008 (2013).
[47]H. Li, T. Goodwill, Z. J. Wang, and L. Ristroph, "Centre of mass location, flight modes, stability and dynamic modelling of gliders," J. Fluid Mech. **937**, A6 (2022).
[48]E. J. Limacher, "Added-mass force on elliptic airfoils," J. Fluid Mech. **926**, R2 (2021).
[49]M. Okamoto, K. Yasuda, and A. Azuma, "Aerodynamic characteristics of the wings and body of a dragonfly," J. Exp. Biol. **199**, 281–294 (1996).
[50]P. Giguère and M. S. Selig, "Low Reynolds number airfoils for small horizontal axis wind turbines," Wind Eng. **21**, 367–380 (1997), available at https://www.scopus.com/record/display.uri?eid=2-s2.0-0031397947&origin=inward&txGid=1c2f589187f69307b97b32302ff3c7f8.
[51]W. A. Timmer and A. P. Schaffarczyk, "The effect of roughness at high Reynolds numbers on the performance of aerofoil DU 97-W-300Mod," Wind Energy **7**, 295–307 (2004).

27 January 2026 08:52:58

© Author(s) 2024